

This article was downloaded by:[MPI Max-Planck-Institute Fuer Quantenoptik]
On: 23 November 2007
Access Details: [subscription number 779599386]
Publisher: Taylor & Francis
Informa Ltd Registered in England and Wales Registered Number: 1072954
Registered office: Mortimer House, 37-41 Mortimer Street, London W1T 3JH, UK



Journal of Modern Optics

Publication details, including instructions for authors and subscription information:

<http://www.informaworld.com/smpp/title~content=t713191304>

Attosecond physics comes of age: from tracing to steering electrons at sub-atomic scales

R. Kienberger^a; M. Uiberacker^b; M. F. Kling^a; F. Krausz^{ab}

^a Max-Planck-Institut für Quantenoptik, D-85748 Garching, Germany

^b Department für Physik, Ludwig Maximilians Universität, D-85748 Garching, Germany

Online Publication Date: 01 September 2007

To cite this Article: Kienberger, R., Uiberacker, M., Kling, M. F. and Krausz, F. (2007) 'Attosecond physics comes of age: from tracing to steering electrons at sub-atomic scales', Journal of Modern Optics, 54:13, 1985 - 1998

To link to this article: DOI: 10.1080/09500340701483170

URL: <http://dx.doi.org/10.1080/09500340701483170>

PLEASE SCROLL DOWN FOR ARTICLE

Full terms and conditions of use: <http://www.informaworld.com/terms-and-conditions-of-access.pdf>

This article maybe used for research, teaching and private study purposes. Any substantial or systematic reproduction, re-distribution, re-selling, loan or sub-licensing, systematic supply or distribution in any form to anyone is expressly forbidden.

The publisher does not give any warranty express or implied or make any representation that the contents will be complete or accurate or up to date. The accuracy of any instructions, formulae and drug doses should be independently verified with primary sources. The publisher shall not be liable for any loss, actions, claims, proceedings, demand or costs or damages whatsoever or howsoever caused arising directly or indirectly in connection with or arising out of the use of this material.

Attosecond physics comes of age: from tracing to steering electrons at sub-atomic scales

R. KIENBERGER*[†], M. UIBERACKER[‡],
M. F. KLING[†] and F. KRAUSZ^{†‡}

[†]Max-Planck-Institut für Quantenoptik, Hans-Kopfermann-Str. 1,
D-85748 Garching, Germany

[‡]Department für Physik, Ludwig Maximilians Universität,
Am Coulombwall 1, D-85748 Garching, Germany

(Received 16 May 2007; in final form 31 May 2007)

Efforts to access ever shorter time scales are motivated by the endeavour to explore the microcosm in ever smaller dimensions. At the turn of the millennium, one and a half decades after the first real-time observation of molecular dynamics with femtosecond laser pulses (1 fs = 10^{-15} s), we witnessed the emergence of sub-femtosecond (that is: attosecond) pulses (1 as = 10^{-18} s). They have been produced in the extreme ultraviolet regime by nonlinear frequency conversion of femtosecond laser pulses. A precise control of the hyperfast electric field oscillations of the driving femtosecond pulses not only allowed the controlled generation of single attosecond pulses and their full characterization but also, for the first time, steering and tracing the atomic-scale motion of electrons.

1. Introductions

Measurement of ever shorter intervals of time and tracing of dynamics within these intervals rely on reproducible generation of ever briefer events and on probing techniques of corresponding resolution [1]. The briefest events produced until recently have been pulses of near-infrared laser light, with durations of around 5 fs (1 fs = 10^{-15} s) [2, 3]. Traditionally, the fastest measurement techniques have used the envelope of these laser pulses for sampling [4]. Recently, sub-femtosecond bunching of femtosecond (>10 fs) extreme ultraviolet light (XUV) was observed in two-colour [5, 6] and two-photon [7] ionization experiments and evidence of sub-femtosecond confinement of XUV emission from few-cycle-driven (ionizing) atoms was also obtained [8]. However, time-domain technique has hitherto not been capable of resolving the time structure of sub-femtosecond transients.

With the event of the stabilization of the carrier-envelope phase of intense few-cycle laser pulses [9] an apparatus was developed that allows reconstruction of atomic processes with a resolution within the Bohr orbit time, which is

*Corresponding author. Email: reinhard.kienberger@mpq.mpg.de

around 150 as. An accurately controlled few-cycle wave of visible light takes ‘tomographic images’ of the time-momentum distribution of electrons ejected from atoms following sudden excitation. From these images the temporal evolution of *both* the emission intensity *and* initial momentum of freed electrons can be retrieved on a sub-femtosecond time scale. Probing primary (photo-excited or collisionally excited) and secondary (Auger) electrons yield insight into, respectively, excitation and subsequent relaxation processes. The transients can be triggered by an isolated attosecond electron or photon burst synchronized to the probing light field oscillations. The technique draws on the basic operation principle of a streak camera [10–14], where a light pulse generates an electron bunch having exactly the same temporal structure. Deflection of the electrons in an electric field allows reconstruction of the duration of the electron bunch. By measuring the temporal evolution of the emission intensity *and* momentum distribution of positive-energy electrons, the atomic transient recorder (ATR) [15] provides direct temporal insight into the rearrangement of the electronic shell of excited atoms on a sub-femtosecond scale.

2. Generation of isolated attosecond pulses

The electric field of linearly-polarized femtosecond laser pulses, if sufficiently strong, induces—in a highly nonlinear interaction—gigantic dipole oscillations by pulling an electron out of the atom and forcing it back towards its core half a cycle later. The oscillations contain high-frequency components extending into the extreme ultraviolet and soft X-ray regimes [2]. In a laser field containing many oscillation cycles, the oscillations are repeated quasi-periodically, resulting in emission of a series of high-energy bursts of sub-femtosecond duration and high-order harmonics of the laser radiation in the spectral domain. For a few-cycle laser driver only a few dipole oscillations, different in amplitude, occur. The oscillation with the highest amplitude has been predicted to produce a single burst in the spectral range of the highest emitted photon energies [16].

With waveform-controlled few-cycle light [9], the few giant atomic dipole oscillations induced can be precisely controlled and reproduced from one laser shot to the next. This is expected to result in an X-ray burst with parameters (duration, energy, timing with respect to the laser field) well reproduced from one shot to the next. Synchronism of the X-ray burst to the field oscillations of the generating laser pulse offers the potential for using the X-ray burst *in combination with* the oscillating laser field for attosecond spectroscopy. This is essential because these laser-produced X-ray bursts are—due to the unfavourable scaling of two-photon transition cross-sections with the photon energy—too weak to be used for *both* triggering *and* probing electronic dynamics (X-ray-pump/X-ray-probe spectroscopy). Instead the oscillating laser field, which changes its strength from zero to maximum within some 600 as in a 750 nm laser wave, can take over the role of the probing X-ray pulse. Experiments have revealed that precise control of the waveform of few-cycle light is an enabling technology for both *controlling* and *tracking* atomic processes on a sub-femtosecond time scale.

3. Measurement of attosecond pulse durations and transients

Inspired by the physics of the first sub-femtosecond experiment [8], Corkum and co-workers [13] put forward the basic concept for ATR metrology, which was analysed with a comprehensive quantum theory by Brabec and co-workers [14]. Let us consider electron emission from atoms exposed to a sub-femtosecond X-ray burst in the presence of an intense, linearly-polarized, few-cycle laser field $E_L(t) = E_0(t) \cos(\omega_L t + \varphi)$ with $E_0(t)$, ω_L and φ_L being the amplitude, frequency and carrier-envelope phase, respectively. The momentum of the freed electrons is changed by $\Delta p = eA_L(t)$ along the laser field vector. Here $A_L(t_r) = \int_{t_r}^{\infty} E_L(t) dt$ is the vector potential of the laser field, and e stands for the charge of the electron, respectively, and t_r is the release time of the electron. This momentum transfer (arrows in figure 1(b)) maps the temporal emission profile into a similar distribution of final momenta $p_f = p_i + \Delta p$ within a time window of $T_0/2 = \pi/\omega_L$, if the electrons' initial momentum p_i is constant in time and their emission terminates within $T_0/2$. Under these conditions the temporal evolution of the electron emission can be unambiguously retrieved from a single 'streaked' momentum distribution (profiles in figure 1(b)).

Streaked spectra recorded at adjacent zero transitions of $A_L(t)$ (indicated with white arrows in figure 2) were analysed and revealed an X-ray pulse duration of $\tau_{x\text{-ray}} = 250(-5/+30)$ as. The temporal intensity profile and chirp of the X-ray pulse obtained from the ATR measurements are shown in the insert of figure 2. The pulse is found to be essentially Fourier-limited (the near-quadratic frequency sweep results

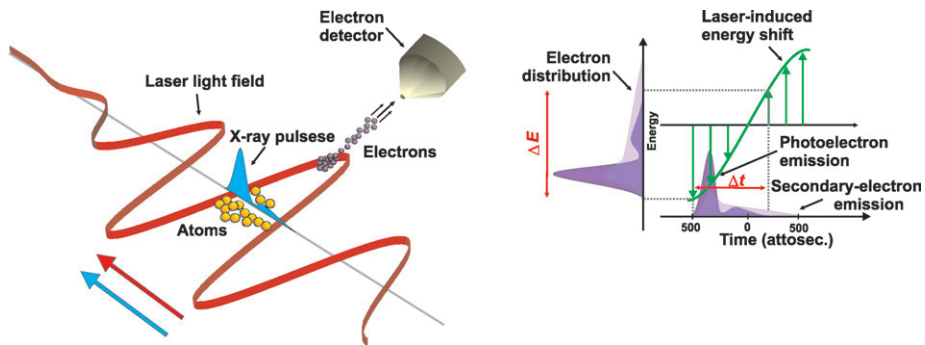


Figure 1. Light-field-controlled streak camera. The dark and light grey curves in (a) represent, respectively, the evolutions of the electric field of the laser light and the intensity of the attosecond X-ray flash. The latter excites the atoms, which then emit electrons. The electrons ejected in the direction of the electric field of the laser light pulse simultaneously beamed in are detected. They undergo, depending on the time of their emission within half the oscillation period of the laser light, a change of velocity: in the case illustrated the electrons emitted first are decelerated, while those released on termination of the X-ray flash are accelerated. In this manner the successively emitted electrons are detected separately. The width ΔE and shape of the measured energy distribution (vertical axis in (b)) of the electrons reflect the duration and evolution of the electron emission, just as their spatial distribution in conventional streak imaging. (The colour version of this figure is included in the online version of the journal.)

from the asymmetric shape of the pulse spectrum rather than from a spectral phase). The remarkable accuracy of $\tau_{x\text{-ray}}$ relies on using several (in this case 3) tomographic projections of the time–momentum distribution of photoelectrons for the X-ray pulse retrieval, which is the essence of the ATR concept. The method is closely related to frequency-resolved optical gating [17–20] with the oscillating field as the gate and other concepts of tomography for ultrashort pulse measurements [21–26].

With isolated sub-femtosecond X-ray pulses at our disposal atomic transients can now be triggered and their subsequent evolution be captured by probing electron emission with a synchronized wave of laser light. In the first ATR measurements presented here, the objects of scrutiny were photoelectrons. The streaking field in these experiments was produced by blocking the internal part of the laser beam with a zirconium filter (transmitting the X-ray pulse) and focusing the transmitted annular beam on the target with the external section of the Mo/Si mirror [9], which can be delayed with respect to the internal section that focuses the X-ray beam.

Figure 2 shows a series of streaked spectra of photoelectrons emitted from neon as a function of Δt . The photoelectron spectrum peaking at $h\omega_{x\text{-ray}} - W_b \approx 72$ eV (where $h\omega_{x\text{-ray}} \approx 93.5$ eV is the centre of the X-ray spectrum selected by the Mo/Si mirror, and $W_b = 21.5$ eV is the binding energy of the most weakly bound valence electrons in Ne) in the absence of the laser field is upshifted by some 10 eV with only a few electrons scattered outside the shifted band.

If the electrons are emitted with an initial kinetic energy much larger than their average quiver energy in the laser field, and temporally confined to a fraction of the half oscillation cycle, theory predicts that their energy shift ΔW is linearly proportional to Δp and hence to the vector potential at the instant of release of the wavepacket, $\Delta W(t_r) \approx (p_i/m)\Delta p(t_r) = (ep_i/m)A(t_r)$, where p_i and m are the initial momentum and the mass of the electron, respectively. As a consequence, $A_L(t)$ and hence $E_L(t)$ can be accurately determined from the peak shifts of the spectra—without having to analyse their detailed structure. The result is shown by the black line in figure 2, constituting the first direct (time-resolved) measurement of a visible light field. From this measurement we can also evaluate the half oscillation period of the electromagnetic field as $T_0/2 \approx 1$ fs. This latter value indicates a significant blue shift to a carrier wavelength of 600 nm near the pulse peak (origin: ionization-induced self-phase modulation in the X-ray source), in agreement with previous observations [9]. With the streaking field $A_L(t)$ known, full temporal (time-momentum) characterization of sub-femtosecond electron emission is now becoming feasible. This capability strictly relies on light waveform control: in its absence the streak records smear out beyond redemption due to irreproducible excitation and probing.

4. Real-time observation of electron tunnelling and multi-electron dynamics in atoms

Atoms exposed to intense light lose one or more electrons and become ions. In strong fields, the process was predicted by Keldysh to occur via tunnelling through the binding potential suppressed by the light field near the peaks of its oscillations. Here, we report on the real-time observation of light-induced electron tunnelling and its potential for studying multi-electron dynamics [27].

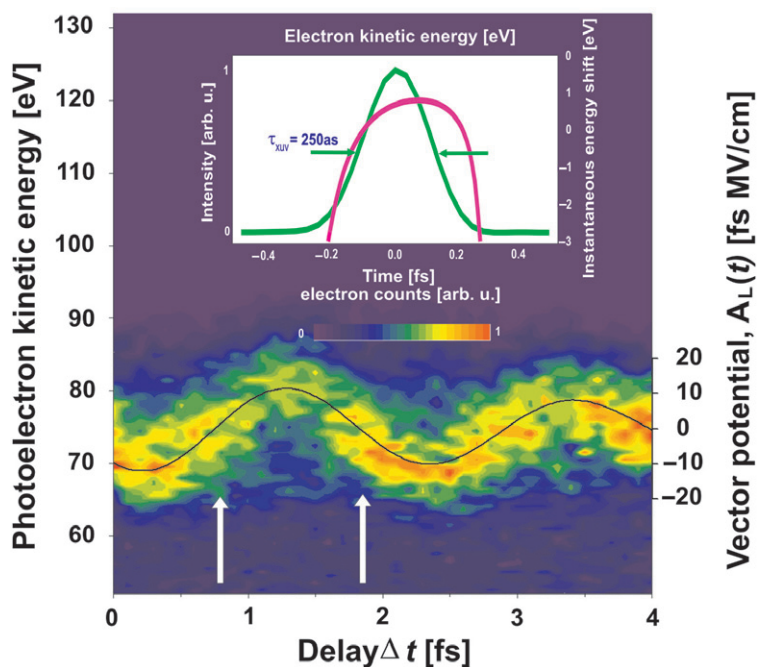


Figure 2. ATR measurement: a series of tomographic projections (streaked kinetic energy spectra) of the initial time-momentum distribution of photoelectrons ejected by a single sub-femtosecond X-ray pulse (in false-colour representation). A few-cycle laser pulse with a cosine waveform and a normalized duration of $\tau_L/T_0 = 2$ was used for both generating the single sub-femtosecond excitation pulse and probing photoelectron emission in the atomic transient recorder. Black line: $A_L(t)$ of the probing field evaluated from the peak shift of the streaked spectra (see scale on the right-hand side). Inset: Temporal intensity profile and energy sweep of the sub-femtosecond X-ray excitation pulse evaluated from the ATR measurements. The basis of the calculation was the unperturbed and two streaked spectra at the zero transitions of the laser electric vector potential marked by the two white arrows. (The colour version of this figure is included in the online version of the journal.)

Keldysh's theory [28] suggested that a valence electron may escape by tunnelling through its atomic binding potential suppressed by the light field. If the dimensionless parameter

$$\gamma = \frac{\omega_L(2mW_b)^{1/2}}{|e|E_0} \quad (1)$$

is less than one, under the assumption of $\hbar\omega_L \ll W_b$ ionization is predicted to be confined to short intervals lasting a fraction of the half oscillation cycle of the light field. Here E_0 and ω_L stand for the amplitude and angular frequency of the oscillations of the laser electric field $E_L(t) = E_0\varepsilon(t) \cos(\omega_L t + \varphi)$, with $\varepsilon(t)$ being the amplitude envelope function, and e , m and W_b are the charge, mass and binding energy of the electron. Recent studies of Yudin and Ivanov suggest that tunnelling remains the dominant ionization mechanism even for γ substantially exceeding one [29].

The temporal evolution of electron emission can be probed by the streaking technique as explained before. Here we want to extend the sampling possibilities by strong-field induced tunnelling unfolding on a sub-femtosecond time scale enabling temporal measurements on the evolution of bound states. Figure 3 illustrates the different options of attosecond sampling of electronic motion in atoms or molecules. The sub-femtosecond XUV pulse triggers the motion by exciting a valence or core electron (figure 3(a), (b), (d) and (e)). The unfolding excitation and relaxation processes lead to photo- or Auger electron emission, which can be probed by the streaking technique using a few-cycle wave of visible or near-infrared (NIR) light with controlled waveform. Bound states involved in the excitation and relaxation cannot be traced by this method. Using the same NIR light wave to ionize these bound electrons by tunnelling ionization within a few sub-femtosecond steps,

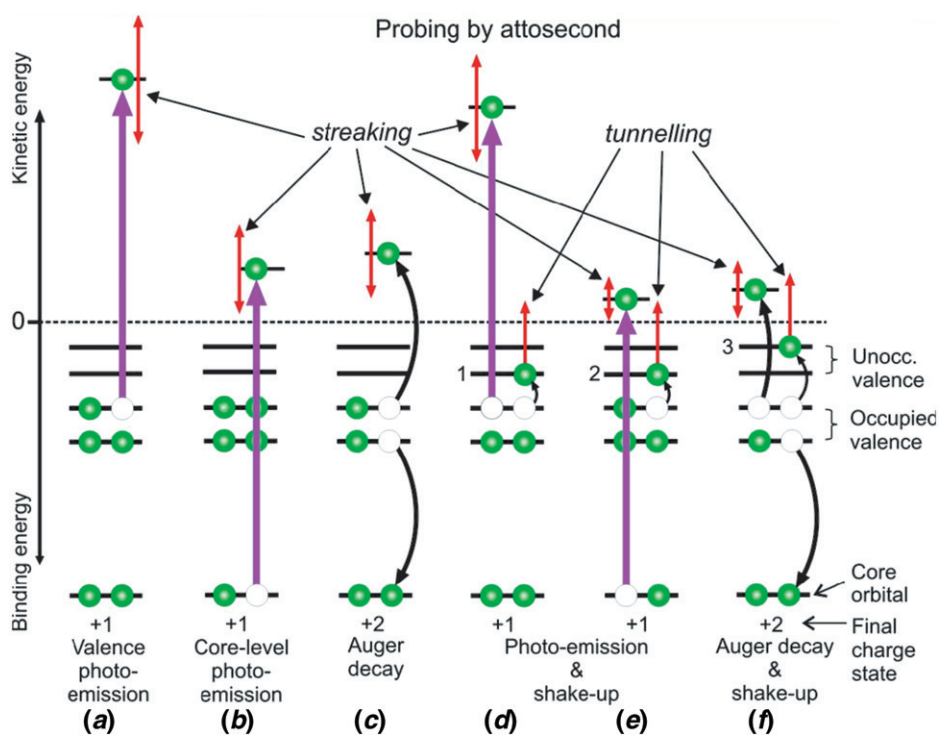


Figure 3. Probing electron dynamics in atoms, molecules or solids with attosecond sampling techniques. A sub-femtosecond XUV pulse triggers the motion by inducing valence (process (a)) or core photoelectron emission (process (b)). The temporal evolution of photo- and Auger electron emission (process (c)) can be probed via attosecond streaking. XUV photoexcitation as well as subsequent Auger decay processes are usually accompanied by shake-up of another electron to a previously unoccupied level (processes (d), (e) and (f)). For sufficiently strong probing laser fields, the shake-up electrons can be liberated by tunnelling ionization. The temporal evolution of the tunnelling current will provide information about the inner-atomic electron dynamics that populate and/or depopulates the interrogated shake-up states. (The colour version of this figure is included in the online version of the journal.)

provides a sub-femtosecond time resolution for probing intra-atomic and intramolecular electron dynamics, including the case that no free electrons are released (*attosecond tunnelling*). This approach relies on the fact that energetic photo-excitation as well as subsequent rearrangement via Auger decay is accompanied by transitions to unoccupied orbitals via shake-up (levels #1, 2 and 3 in figure 3 (d)–(f)). The term ‘shake-up’ stands here for all possible processes populating excited ionic states (including both instantaneous as well as non-instantaneous ones). These populations can be probed via optical field ionization by a strong, few-cycle NIR pulse of variable delay, Δt , with respect to the sub-femtosecond XUV excitation by measuring the number of ions resulting from the XUV-pump/NIR-probe exposure as a function of Δt .

Shake-up usually populates several quantum states in the valence band, from which electrons can be freed by the NIR probe. Hence, the ion yield will constitute an integral signal, with contributions from all shake-up states up to a certain binding energy from which ionization is feasible for the intensity chosen. Population dynamics of individual states of significantly differing binding energy can be retrieved by pump–probe scans repeated at different NIR probe intensities and/or from the temporal separation of the depletion of the states in one and the same delay scan. The ion yield constitutes an integral signal in a temporal sense, too. The shake-up states are exposed to the ionizing NIR field from the moment they have been populated until the end of the NIR pulse. As the delay is scanned from large negative values (negative stands for: NIR-probe comes first) to large positive values (XUV-pump first) the measured ion yield starts increasing at $\Delta t < 0$ due to ionization on the trailing edge of the NIR pulse and continues to increase with increasing Δt owing to the XUV pump shifting towards the peak of the ionizing NIR probe and having the shake-up states exposed to ever higher NIR probe intensities.

The time-dependent ionization dynamics can be traced by measuring the yield of ions of different charges as a function of the delay between the XUV pump and the sampling NIR light field. With a sufficiently rapid ($\ll 1$ fs) excitation, these measurements can thus provide direct insight into the temporal evolution of shake-up (in the presence of a strong optical field) and light-induced tunnelling. We have proven this concept by first experiments on neon and xenon atoms exposed to our sub-femtosecond XUV pump and few-cycle NIR probe pulses. The experiments have been performed with waveform-controlled laser pulses with a duration of $\tau_L \sim (5.5 \pm 0.5)$ fs, at a repetition rate of 3 kHz. The laser pulses produce sub-femtosecond XUV pulses. Both, laser and XUV pulses are focused onto an atomic gas target. Ions created in the common focus of the two beams are detected by a (reflectron type) time-of-flight ion spectrometer.

5. Shake-up and tunnelling

For probing shake-up and light-induced electron tunnelling neon atoms have been studied. The core shell was not accessed by the 91 eV XUV photons used here, hence Auger decay is absent. The threshold energies for single and double ionization from the outer shell of Ne are 21.56 and 62.53 eV, respectively—both accessible with

the current photon energy. As a consequence Ne^{1+} and Ne^{2+} ions are produced with a ratio of $(19.7:1) \pm 0.5$ by the XUV light. A few percent of the Ne^{1+} ions are promoted into $2p^{-2}nl$ ($n: 3, 4; l: s, p, d$) configurations. These satellite states can only decay radiatively on a picosecond time scale.

Adding the NIR probing field increased the yield of Ne^{2+} for a delay $\Delta t \ll -\tau_L$. The total NIR-induced Ne^{2+} yield enhancement amounted to $(40 \pm 4)\%$ of the XUV-produced Ne^{2+} yield at a NIR peak intensity of $(7 \pm 1) \times 10^{13} \text{ W cm}^{-2}$. The absence of this enhancement for $\Delta t \ll -\tau_L$ clearly indicates that the laser sets electrons free from states excited by the XUV pulse. A substantial fraction of the population of the $2p^{-2}nl$ shake-up satellites is freed by tunnelling ionization.

Figure 4(a) shows the number of Ne^{2+} ions detected as a function of delay Δt between the XUV pump and NIR probe. Figure 4(b) compares the experimental data (squares) with the theoretical prediction (lines) based on the Keldysh theory (refined by Yudin and Ivanov [29]). The calculations are in reasonable agreement with our measurements and reveal how the different shake-up states are depleted sequentially by laser-field ionization. States in configurations $2p^{-2}4p$ and $2p^{-2}3d$ are depleted already at negative delays (where the intensity is still low) and $2p^{-2}3p$ and $2p^{-2}3s$ states, which constitute approx. 75% of all shake-up states and have relatively high binding energies (~ 10 and 13 eV , respectively) at around zero delay. The latter are depleted within approximately one and a half wave cycles of the NIR field, where the laser intensity has increased sufficiently. Several sharp steps that are spaced by $\sim T_L/2$ can be seen in this region, giving a clear indication of field-induced tunnelling being dominantly responsible here. This conclusion is also supported by the disappearance of the steps in a pump-probe scan performed with a randomly varying carrier-envelope phase of the NIR probe pulses (grey line in figure 4(a)). Although the Keldysh parameter γ is of the order of 3 in this experiment, the steps appear in the data. Hence, the experiment verifies not only the existence of light-field-induced tunnelling, as predicted by Keldysh some four decades ago, but also confirms the dominant role of this ionization mechanism up to γ values substantially exceeding 1.

The steepness of the ionization steps and the dips preceding them in the measured data are not well reproduced by our model, which neglects the influence of electron-electron interactions and that of the strong NIR field on the XUV-induced transitions populating the shake-up states. Apart from these discrepancies the experiment provides for the first time profound insight into fundamental electronic processes such as tunnelling and shake-up by contrasting theoretical models with time-domain data. Currently, the observed sub-400 as rise time of the Ne^{2+} yield (which sets a corresponding upper limit on the time it takes the excited electronic states to become populated during XUV ionization and on tunnelling), see inset in figure 4(a), dictates the temporal resolution being achievable. After refining the experimental accuracy as well as the theoretical modelling this technique will allow determination of the attosecond temporal evolution of the light-field-induced tunnelling current and will provide more insight into the nature of e^-e^- interactions responsible for shake-up. Electrons are found to escape from their atomic binding potential within several sub-femtosecond time intervals near the oscillation peaks of the ionizing few-cycle near-infrared laser field. The observed sub-femtosecond

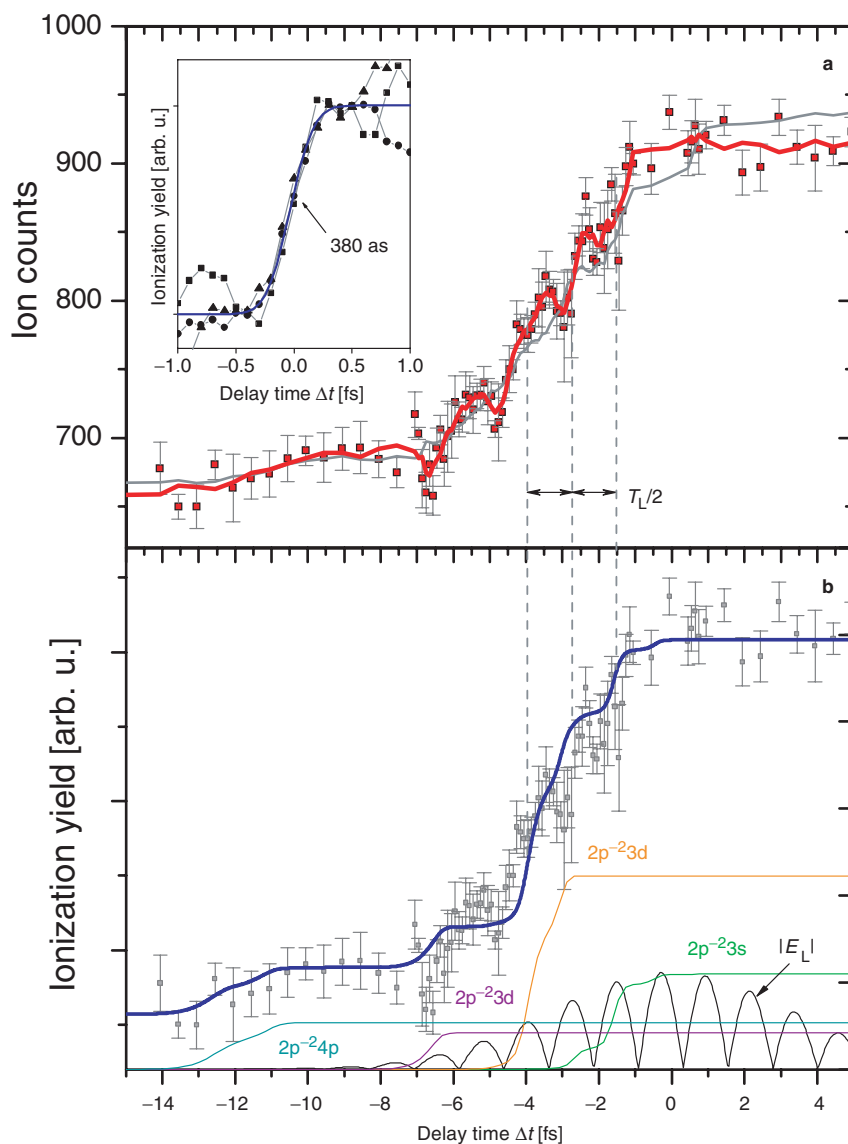


Figure 4. Ne^{2+} ion yield versus delay: experiment and modelling. (a) The squares and the error bars show the average and the standard deviation of the measurements. Thick red line: the average of 5 adjacent data points; thin grey line, the same as the thick line but recorded with NIR probe pulses of random carrier-envelope phase. Inset: Squares, triangles, and circles depict an ionization step extracted from 3 different measurements normalized to give the same change in the ionization yield. Solid line: error-function fit with a rise time of 380 as. (b) The thin solid lines show the calculated fractional ionization yields contributed by electrons liberated from different shake-up states. The thick solid line depicts the overall ionization rate obtained by totalling the fractional rates. The simulations were carried out for a Gaussian 250 as XUV pulse and a Gaussian 5.5 fs laser pulse with a peak intensity of $7 \times 10^{13} \text{ W cm}^{-2}$. The black solid curve represents the modulus of the NIR laser electric field $|E_L|$. (The colour version of this figure is included in the online version of the journal.)

ionization steps provide a powerful means of probing the transient population of short-lived valence electronic states in excited atoms or molecules, offering direct, time-domain access to a wide range of multi-electron dynamics unfolding on an attosecond to femtosecond time scale. Simultaneous implementation of attosecond tunnelling and attosecond streaking spectroscopy along with scaling of the techniques to higher photon energies and shorter X-ray pulse durations will provide unprecedented insight into the transient electronic states of matter.

6. Sub-femtosecond control of electron dynamics

The generation of attosecond pulses and their complete characterization [15] demonstrate the capability of steering the motion of electrons inside and around atoms with strong light fields [30]. These achievements have provoked the question, whether light-field control of electron motion [31] can be extended to more complex systems, such as electron wave packet motion in simple molecules and possibly even electron motion in complex (bio)molecules and nanosystems.

Control of chemical reactions or photo-biology has been previously achieved by employing laser pulses as photonic reagents [32], with their duration, intensity, frequency, chirp, and polarization being used as control parameters. The introduction of laser light with a stable and synthesized evolution of the electric field $E(t) = E_0(t) \cos(\omega t + \varphi)$, adds new functionality to photonic reagents that can be used to control electron motion.

First experimental evidence that electron motion can be controlled by synthesized light waveforms was obtained recently in the strong-field dissociation of the hydrogen molecule, being one of Nature's most simple molecular systems. H_2 (along with its isotopes HD and D_2) has been the subject of many experimental and theoretical research efforts and many of the processes in terms of which strong-field molecular interactions are presently interpreted (bond softening, enhanced ionization, etc.) were discovered in experimental and theoretical work on this molecule. It has furthermore been the testing ground for several exciting experimental approaches such as 'molecular clock' experiments that are based on correlated electronic and nuclear motion [33, 34].

Following the proposal of Haljan *et al.* [35], we have ionized D_2 with waveform-controlled few-cycle laser pulses [36]. Detailed previous studies have revealed several pathways in the dissociation of H_2 , HD and D_2 in intense laser fields whose relative importance depends on intensity and pulse duration [37]. In the double ionization of these systems, two momentum-matched ions are produced that are symmetrically emitted along the molecular axis, irrespective of the evolution of the driving fields. Light-waveform control of the dissociation of D_2 thus requires double ionization to be kept at a minimum. We utilized the velocity-map imaging technique [38] to monitor the emission of D^+ ions from the dissociation of D_2 , allowing us to identify the fragmentation channels by their characteristic energy and angular distributions. The carrier-envelope phase served as a control parameter for the electric field waveform.

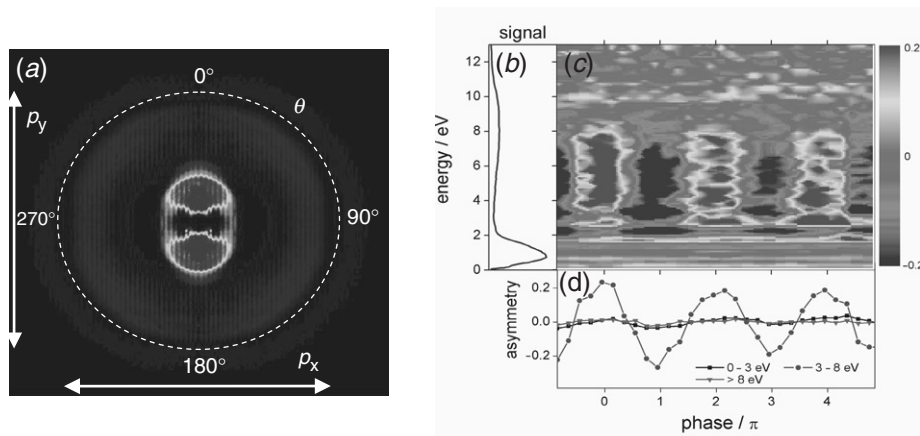


Figure 5. (a) Two-dimensional D^+ momentum image for D_2 dissociation in a 5 fs, $1 \times 10^{14} \text{ W cm}^{-2}$ laser field with randomly varying phase (the laser polarization is vertical); (b) D^+ kinetic energy spectrum derived from (a); (c) asymmetry of the D^+ ion emission along the laser polarization (integrated over an angular range of 60°) as a function of the D^+ kinetic energy and carrier envelope phase π ; (d) asymmetry integrated over several energy ranges. (The colour version of this figure is included in the online version of the journal.)

Figure 5 (a) shows a cut through the D^+ 3D-momentum distribution in Cartesian coordinates (p_x, p_y) at $p_z = 0$, for a 5 fs, $1 \times 10^{14} \text{ W cm}^{-2}$ laser field with a randomly varying phase φ . The laser was polarized along the y axis ($\theta = 0^\circ/180^\circ$). The kinetic energy spectrum derived from the image is displayed in figure 5 (b). According to previous studies [39], the contributions in the centre of the image, which show relatively narrow angular distributions, can be attributed to bond softening (0–2 eV) and a weak enhanced ionization channel (2–3 eV). A nearly isotropic distribution is measured for higher energies (between 3 and 10 eV) and is a typical signature of fragmentation induced by electron recollision [40] (with the electron that is emitted upon ionization of D_2), being further supported by its absence with circular instead of linear polarized laser pulses.

No difference in the up versus down emission of D^+ ions (along the laser polarization axis) is observed with a randomly varying phase. Figure 5 (c) reveals how phase locking (and thus stabilization of the waveform of the laser electric field) results in a non-zero asymmetry

$$A(W, \varphi) = \frac{P_{\text{up}}(W, \varphi) - P_{\text{down}}(W, \varphi)}{P_{\text{up}}(W, \varphi) + P_{\text{down}}(W, \varphi)}$$

of the ion yields $P_{\text{up}}(W, \varphi)$ and $P_{\text{down}}(W, \varphi)$ in the up and down directions, respectively, as a function of the kinetic energy W of the D^+ fragments and the laser phase φ . Regions in figure 5 (c) where the asymmetry oscillates as a function of the phase represent conditions where the direction of the D^+ emission—and hence the localization of the electron in the dissociation process—is effectively controlled by the sub-cycle evolution of the laser field driving the dissociation. The extent of the control is further illustrated in figure 5 (d), which displays a series of curves where the asymmetry is integrated over selected energy intervals. The highest degree

of asymmetry with a modulation depth of ca. 50% is observed between 3 and 8 eV, indicating the important role of electron recollision for the observed control of the directional D^+ emission.

To further understand the mechanism of the light-field control of the D_2 fragmentation, we have modelled the laser-driven motion of the two nuclei and the bound electron by numerically solving the time-dependent Schrödinger equation. To simplify the theoretical treatment, D_2 is assumed to be aligned along the laser polarization axis and is ionized at the maximum of the laser electric field, producing an electron wave packet and a vibrational wave packet in the $1s\sigma_g^+$ ground electronic state of D_2^+ . Electron recollision (introduced in our model at a delay of 1.7 fs after ionization, corresponding to the first recollision time [33]) leads to excitation from the $1s\sigma_g^+$ ground electronic state to the $2p\sigma_u^+$ excited electronic state. The time evolution of the wavefunction for the D_2^+ molecule after recollision is calculated by expanding the full wavefunction for the electronic coordinate (\mathbf{r}) and the internuclear distance R in terms of the two lowest-lying electronic states, i.e.

$$\Psi(\mathbf{r}, R; t) \approx |1s\sigma_g\rangle\psi_g(R; t) + |2p\sigma_u\rangle\psi_u(R; t), \quad (2)$$

where $\psi_{g/u}(R; t)$ represent the nuclear wave packets corresponding to the $1s\sigma_g^+$ and $2p\sigma_u^+$ states (for the full theoretical treatment, see [36]).

Due to the repulsive nature of the $2p\sigma_u^+$ state, dissociation via this state can result in a large kinetic energy (up to ca. 10 eV) of the D^+ and D fragments. During the dissociation, the laser field transfers part of the $2p\sigma_u^+$ population back to the $1s\sigma_g^+$ state, producing a dissociative wave packet with a large excess kinetic energy. The emerging coherent superposition of the two electronic states results in a time-dependent localization of the electron density on the upper or lower nucleus [41]. The calculated time-dependent localization of the electron density in D_2^+ is shown in figure 6(a) together with the corresponding laser waveforms for cosine and $-\cosine$ shaped pulses).

The electron density oscillates between the upper and lower nucleus as the internuclear distance increases. Beyond a critical internuclear distance, the electron can no longer tunnel through the potential barrier emerging between the two nuclei and remains on the upper nucleus for a cosine-shaped pulse in figure 6(a). At which one of the two nuclei the electron remains is determined by the phase of the oscillatory electron motion relative to the dissociation time. In agreement with our experimental observation, a shift of the carrier-envelope phase φ by π turns the direction of emission of the ionic/atomic fragment opposite (as shown in figure 6(a)).

The mechanism for the observed control of the electron localization in D_2^+ and its dissociation is summarized in figure 6(b). The observation of asymmetric D^+ emission as a result of electron localization requires that we are unable to identify the quantum path (i.e. the $1s\sigma_g^+$ or the $2p\sigma_u^+$ curve) along which the measured ions were created. This restricts the kinetic energy range where an asymmetric emission may be expected. Electron localization is calculated to peak around 6 eV, in good agreement with the experimentally observed asymmetry.

This experiment demonstrates that (i) attosecond electron motion is relevant to chemical processes, and (ii) attosecond shaping of the light field in a *femtosecond* pulse can be used to control it. The results reviewed here are first examples of the

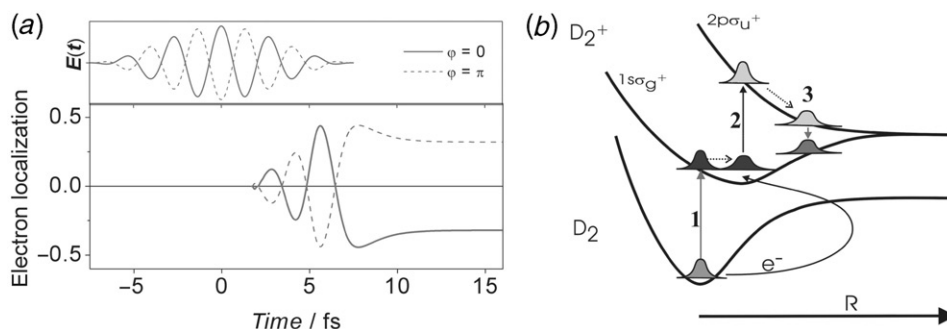


Figure 6. (a) Evolution of the electric field of the 5 fs pulse corresponding to a cosine-shaped ($\varphi = 0$) and a $-\cosine$ -shaped ($\varphi = \pi$) waveform (top) and calculated evolution of the electron localization according to the model described in the text for the two waveforms with $\varphi = 0$ (solid line) and $\varphi = \pi$ (dashed line). (b) Three-step mechanism for the creation of the observed asymmetry in the D_2 fragmentation: (1) ionization of D_2 , (2) excitation of D_2^+ via electron recollision and (3) preparation of a coherent superposition of the $1s\sigma_g^+$ and $2p\sigma_u^+$ states. (The colour version of this figure is included in the online version of the journal.)

control of intra-molecular electronic motion and may provide a first clue for the control of intra-molecular electron transfer processes by synthesized light fields in more complex systems.

Acknowledgements

We gratefully acknowledge the invaluable contributions of E. Goulielmakis, M. Schultze, V. Yakovlev, Th. Uphues, A.J. Verhoef (MPQ), A. Baltuska, A. Scrinzi (TU Vienna, A), U. Kleineberg, U. Heinzmann (Uni Bielefeld, D), M. Drescher (Uni Hamburg, D), and M.J.J. Vrakking (AMOLF, NL) to the experiments reviewed in this paper. This research was supported by the DFG cluster of excellence Munich Centre for Advanced Photonics (www.munich-photonics.de). MFK acknowledges support from the DFG Emmy-Noether program.

References

- [1] A. Zewail, *J. Phys. Chem. A* **104** 5660 (2000).
- [2] T. Brabec and F. Krausz, *Rev. Mod. Phys.* **72** 545 (2000).
- [3] U. Keller, *Nature* **424** 831 (2003).
- [4] M. Drescher, M. Hentschel, R. Kienberger, *et al.*, *Science* **291** 1923 (2001) [published online February 15, 2001; 10.1126/science.1058561].
- [5] P.M. Paul, E.S. Toma, P. Breger, *et al.*, *Science* **292** 1689 (2001).
- [6] Y. Mairesse, A. de Bohan, L.J. Fransink, *et al.*, *Science* **302** 1540 (2003).
- [7] P. Tzallas, D. Charalambidis, N.A. Papadogiannis, *et al.*, *Nature* **426** 267 (2003).
- [8] M. Hentschel, R. Kienberger, C. Spielmann, *et al.*, *Nature* **414** 509 (2001).
- [9] A. Baltuska, T. Udem, M. Uiberacker, *et al.*, *Nature* **421** 611 (2003).
- [10] C. Wheatstone, *Phil. Mag.* **6** 61 (1835).
- [11] D.J. Bradley, B. Liddy and W.E. Sleat, *Opt. Commun.* **2** 391 (1971).

- [12] M. Schelev, M.C. Richards and A.J. Alcock, *Appl. Phys. Lett.* **18** 354 (1971).
- [13] J. Itatani, F. Quere and G.L. Yudin, *Phys. Rev. Lett.* **88** 173903 (2002).
- [14] M. Kitzler, N. Milosevic, A. Scrinzi, *et al.*, *Phys. Rev. Lett.* **88** 173904 (2002).
- [15] R. Kienberger, E. Goulielmakis, M. Uiberacker, *et al.*, *Nature* **427** 817 (2004).
- [16] I.P. Christov, M.M. Murnane and H.C. Kapteyn, *Phys. Rev. Lett.* **78** 1251 (1997).
- [17] D.J. Kane and R. Trebino, *IEEE J. Quantum Electron.* **29** 571 (1993).
- [18] T. Sekikawa, T. Katsura, S. Miura, E. Goulielmakis, M. Uiberacker, *et al.*, *Phys. Rev. Lett.* **88** 193902 (2002).
- [19] M. Vampouille, A. Barthelemy, B. Colombeau, *et al.*, *J. Opt. (Paris)* **15** 385 (1984).
- [20] M.T. Kaufman, W.C. Banyai, A.A. Godil, *et al.*, *Appl. Phys. Lett.* **64** 270 (1994).
- [21] M. Beck, M.G. Raymer, I.A. Walmsley, *et al.*, *Opt. Lett.* **18** 2041 (1993).
- [22] I. Walmsley, *et al.*, *J. Opt. Soc. Am B* **13** 2453 (1996).
- [23] C. Dorrer and I. Kang, *Opt. Lett.* **28** 1481 (2003).
- [24] M. Drescher, M. Hentschel, R. Kienberger, *et al.*, *Nature* **419** 803 (2002).
- [25] A. L'Huillier and P. Balcou, *Phys. Rev. Lett.* **70** 774 (1993).
- [26] J.J. Macklin, J.D. Kmetec and C.L. Gordon III, *Phys. Rev. Lett.* **70** 766 (1993).
- [27] M. Uiberacker, T. Uphues, M. Schultze, *et al.*, *Nature* **446** 627 (2007).
- [28] L.V. Keldysh, *Sov. Phys. JETP* **20** 1307 (1965).
- [29] G.L. Yudin and M.Yu. Ivanov, *Phys. Rev. A* **64** 013409 (2001).
- [30] E. Goulielmakis, M. Uiberacker, R. Kienberger, *et al.*, *Science* **305** 1267 (2004).
- [31] M. Kitzler, K. O'Keeffe and M. Lezius, *J. Mod. Opt.* **53** 57 (2006).
- [32] H. Rabitz, *Science* **299** 525 (2003).
- [33] H. Niikura, F. Legare, R. Hasbani, *et al.*, *Nature* **417** 917 (2002).
- [34] H. Niikura, F. Legare, R. Hasbani, *et al.*, *Nature* **421** 826 (2003).
- [35] P. Haljan, M.Y. Ivanov and P.B. Corkum, *Laser Phys.* **7** 1 (1997).
- [36] M.F. Kling, C. Siedschlag, A.J. Verhoef, *et al.*, *Science* **312** 246 (2006).
- [37] J.H. Posthumus, *Rep. Prog. Phys.* **67** 623 (2004).
- [38] A.T.J.B. Eppink and D.H. Parker, *Rev. Sci. Instrum.* **68** 3477 (1997).
- [39] K. Sändig, H. Figger and T.W. Hansch, *Phys. Rev. Lett.* **85** 4876 (2000).
- [40] A.S. Alnaser, X.M. Tong, T. Osipou, *et al.*, *Phys. Rev. Lett.* **93** 183202 (2004).
- [41] A.D. Bandrauk, S. Chelkowski and H.S. Nguyen, *Int. J. Quant. Chem.* **100** 834 (2004);
H. Niikura, D.M. Villeneuve and P.B. Corkum, *Phys. Rev. A* **73** 021402 (2006);
G.L. Yudin, S. Chelkowski, J. Itatani, *Phys. Rev. A* **72** 051401 (2006).